Nonadiabatic Control of a Superconducting Qubit via Strong Driving

by

Matthew W. Farrell

Submitted to the Department of Physics
in partial fulfillment of the requirements for the degree of

Bachelor of Science in Physics

at the

MASSACHUSETTS INSTITUTE OF TECHNOLOGY

June 2008

MASSACHUSETTS INSTITUTE OF TECHNOLOGY
JUN 13 2008
LIBRARIES

ARCHIVES

© Matthew W. Farrell, MMVIII. All rights reserved.

The author hereby grants to MIT permission to reproduce and distribute publicly paper and electronic copies of this thesis document in whole or in part.

Author ....
Department of Physics
May 8, 2008

Certified by..........................
Leonid Levitov
Professor of Physics
Thesis Supervisor

Accepted by ....
David E. Pritchard
Senior Thesis Coordinator, Department of Physics

Nonadiabatic Control of a Superconducting Qubit via Strong Driving

by

Matthew W. Farrell

Submitted to the Department of Physics
on May 8, 2008, in partial fulfillment of the
requirements for the degree of
Bachelor of Science in Physics

Abstract

Quantum computation offers the promise of speeding up many calculations that are intractable on classical computers, including but not limited to factoring and the simulation of quantum mechanical systems. Quantum computation is achieved by replacing the bits of a classical computer with qubits. Qubits generalize bits by allowing not only the classical states of zero and one, but also any arbitrary superposition of zero and one. These qubits are implemented as two-state systems by mapping the classical one and zero states to two orthogonal quantum states. The qubits are then manipulated by varying the Hamiltonian of the two-state systems with time. The standard method to manipulate a two-state system is to drive it weakly using Rabi dynamics. This approach is ineffective for a large scale quantum computer because the rotation is slow, and decoherence breaks the fragile state before the computation can be completed. To address this problem, we developed a method to rapidly rotate a qubit by an arbitrary angle. This is achieved by abandoning Rabi oscillations, and instead using a strong, rapidly changing field to coherently rotate the spin. We rapid drive the system through an avoided crossing and back again by giving the on diagonal term of the Hamiltonian a parabolic time dependence. In this paper, I contrast the standard method of spin rotation via Rabi oscillations with our protocol. Then, I discuss the various numerical simulations used to evaluate our protocol. Finally, I present some experimental evidence suggesting the protocol will be effective when implemented. Then, I discuss experimental findings and computational results of our method.

We found regions of parameter space that allow a qubit to be rapidly rotated by any angle from zero to nearly π. This new protocol for arbitrary qubit rotation is a significant improvement over techniques relying on Rabi oscillations, reducing the time needed to transition qubits. Our protocol deserves further study and refinement for its potential to speed up and, thusly, reduce the problem of decoherence in quantum computation.

Thesis Supervisor: Leonid Levitov
Title: Professor of Physics

Acknowledgments

First and foremost I would like to thank Professor Leonid Levitov and Mark Rudner for their help throughout the project. This work would not have been possible without their ideas and suggestions or the time they took to help me understand the underlying physics and mathematics.

Next I would like to thank my familly for their constant support throughout my time at MIT.

Finally, I would like to thank the Paul E. Gray Endowed Fund for UROP, which made this work possible.

Contents

1 Introduction 11

1.1 Quantum Computation 11

1.2 The Superconducting Flux Qubit 12

1.3 Comparison to Weak Driving 14

2 Background 15

2.1 Theory 15

2.2 Rotating Frame 18

2.3 Experimental Setup 19

3 Protocol 23

3.1 Simulation 23

3.1.1 Transition Probability vs. Time 24

3.1.2 Bloch Vector vs. Time 24

3.1.3 Transition Probability vs. Detuning and Amplitude 25

3.1.4 Transition Probability vs. Detuning 27

3.1.5 Final Bloch vector vs. Detuning 27

3.1.6 Transition Probability vs. Time and Detuning 28

3.2 Experiment 28

3.3 Pulse Shape Variations 30

4 Conclusion 33

A MATLAB Scripts 35

A.1 evolve.m 35

A.2 final.m 37

A.3 contour.m 38

A.4 rotbloch.m 39

List of Figures

1-1 Schematic of a experimental setup. Inner box is qubit, Xs representing Josephson junctions. Outer box is a SQUID, used to measure the state of the qubit. Inductors on left generate magnetic field to control Hamiltonian. 13

2-1 Systems starts in $|0\rangle$ on the lower right leg. It is then driven through the avoided crossing twice before returning to original location. 16

2-2 A and B show the first and second eigenstates of a symmetric potential with a double harmonic well. Note how each takes the form of a pair of Gaussians. C and D show the first and second eigenstates of an asymmetric double harmonic well. Note how each is a single, localized Gaussian. 20

3-1 z component of ψ vs. time for two detunings. Note how dynamics only occur when ϵ is small (off scale, ϵ continues quadratically) 24

3-2 Time evolution of Bloch vector for 3 detunings. Three views of the same time evolutions, just from different angles. 25

3-3 Final value of z component of ψ vs. Amplitude and the ratio of detuning to amplitude. Spin is fully flipped at $(1.585 \pm .005, 0.9765 \pm .00025)$ and $(3.464 \pm .005, 0.9960 \pm .00025)$ 26

3-4 Final value of z component of ψ vs. detuning for two amplitudes. Note the range extends to -1 in both, indicating a full π rotation. 27

3-5 Final value of Bloch vector vs. detuning. All three figures show the same plot but from different angles. 28

3-6 Experimental results. Detuning (y-axis) and time (x-axis) against transition probability (color) 29

3-7 Simulation results. Detuning (y-axis) and time (x-axis) against transition probability (color). Note that colors are reversed relative to experimental plot 29
3-8 Final value of z component of ψ vs. Amplitude and the ratio of detuning to amplitude. Here driven by a true cosine waveform 31
3-9 Final value of z component of ψ vs. Amplitude and the ratio of detuning to amplitude. Here driven by a triangular waveform. 31

Chapter 1

Introduction

Quantum computation holds much promise for physics, but several major technical hurdles must be overcome in order to implement a quantum computer. Some of these problems are overcome by superconducting flux qubits, but others persist. One major problem is decoherence, which is exacerbated by the long time needed to manipulate qubits using Rabi oscillations, the current standard. We present a new protocol based on strong resonant driving which will reduce the time needed to manipulate bits.

1.1 Quantum Computation

Quantum computation will, if realized, significantly improving our ability to understand physical systems. Often overlooked for its near tautology, one of the most promising uses of quantum computation is to model quantum mechanical systems [4]. Since a quantum mechanical system can enter superpositions of its basis states, the number of possible states of a quantum system increases exponentially with the number of basis states. Thus classical computers, unable to enter superpositions, must use an exponentially large amount of space and time to simulate quantum mechanical systems relative to the size of the quantum system. This exponential growth makes all but simple quantum mechanical systems intractably difficult to simulate on a classical computer.

Just as classical computers reduce computations to problems representable by bits, quantum computers reduce problems to qubits. Each qubit is a two-state system. While bits may only be in two states, one or zero, qubits my be in any superposition of their two states, any superposition of one and zero. A convenient example of a two-state system is a spin-1/2 particle, which has as its two states spin-up and spin-down. While dynamically equivalent to any other two-state system, the spin-1/2 particle is easily visualized in terms of the Bloch sphere [5]. Thus, in this paper I will frequently describe two-state systems in terms of spin-1/2 particles and the Bloch sphere models, describing changes in state as rotations.

Quantum computers are immune from the difficulty classical computers face in simulating quantum systems. As they themselves are quantum systems, quantum computers can also enter superpositions. Hence, quantum computers may also represent an exponentially large number of superpositions, making the calculation tractable. However, this power comes at a price. Superimposed states of current quantum computers are incredibly fragile, breaking easily from any interaction [3]. Furthermore, current methods of manipulating the state of quantum computers rely on Rabi oscillation. Rabi oscillations, though coherent, rely on a weak coupling between the quantum system and the dynamic terms of the Hamiltonian, so they are slow. Slow interaction implies long interaction time and a high probability for decoherence.

We attempt to address the problem of decoherence by proposing a new protocol for manipulating two-state systems. Before delving further into the goal, I will first discuss the target platform.

1.2 The Superconducting Flux Qubit

A promising resource for the construction of a quantum computer is the superconducting persistent-current qubit [7]. Persistent-current qubits are designed to quantize the current states such that there is no state with zero current. Hence, even the minimum energy state has either a clockwise of anticlockwise persistent current. These current couple to any external magnetic fields, allowing the energy gap between states to be tuned by varying the applied magnetic field. Cooling reduces thermal fluctuations, confining the system to only the lowest energy states. The system may then be approximated well as a two state system, ignoring all states save the ground state and first excited state. The energy gap between these two states can be set by varying the applied longitudinal magnetic field, while the mixing energy is a constant for the system [6]. In summary, we studied the dynamics of a two-state system with a

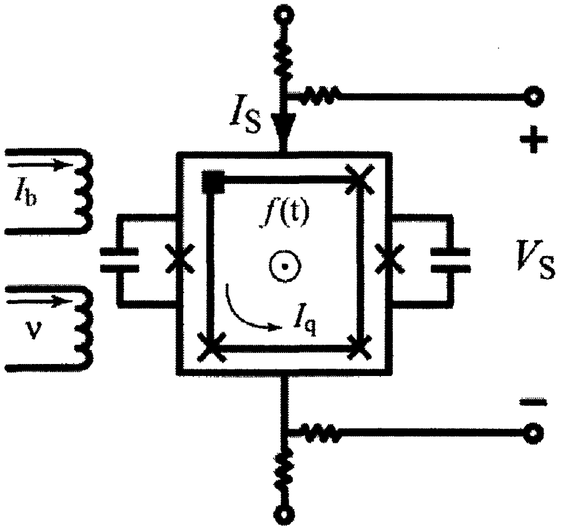

Figure 1-1: Schematic of a experimental setup. Inner box is qubit, Xs representing Josephson junctions. Outer box is a SQUID, used to measure the state of the qubit. Inductors on left generate magnetic field to control Hamiltonian.

variable energy gap and a fixed mixing energy, represented by the Hamiltonian

$$H(t) = \begin{pmatrix} \epsilon(t) & \Delta \\ \Delta & -\epsilon(t) \end{pmatrix} \tag{1.2.1}$$

Experimentally, it is easiest to vary the magnetic field sinusoidally via rf-radiation, so we focus on the following special case.

$$\epsilon(t) = \epsilon_0 + A_{rf} \cos \omega t \tag{1.2.2}$$

Returning to the goal of minimizing interaction time, a natural time scale is inherent to our Hamiltonian. First, note that any real computation will require multiple steps, so for each step the applied field should complete a closed loop through parameter space.

We now have three features to consider in choosing how to vary the magnetic field to rotate the qubit: minimize time to minimize decoherence, sinusoidal is easy experimentally, and complete a closed loop through parameter space so multiple operations can be chained. The most natural way to achieve all three is to realize a rotation via a single sinusoidal cycle of the imposed magnetic field.

1.3 Comparison to Weak Driving

There already is a way to achieve arbitrary rotations of a qubit, namely Rabi oscillation under weak driving. Our method is only an improvement if, in addition to being capable of performing arbitrary rotations, it also provides a speed improvement over weak driving.

The time scale for our method is extremely easy to calculate: one cycle of the driving field. Based on the results of this work, we will see the frequency of the driving field should be on the order of $\Delta/\hbar$.

Rabi oscillations rely on Larmor Precession, which occurs at a frequency given by $\nu = (A_{rf} \sin 2\theta)/h$, where θ is defined with $\tan 2\theta \equiv \Delta/E$ [2]. Thus we see that the frequency is determined by both the parameters of the system and the maximum driving magnetic field. Since the driving magnetic field must be oscillating at the Larmor frequency of the unperturbed system, it generally needs to be in the mega- to gigahertz range, making it difficult to additionally have a large amplitude.

Chapter 2

Background

2.1 Theory

I begin by mapping the classical one and zero states to the eigenstates of $\hat{\sigma}_z$.

$$|0\rangle \equiv \begin{pmatrix} 1 \\ 0 \end{pmatrix} \equiv 0_{classical} \tag{2.1.1}$$

$$|1\rangle \equiv \begin{pmatrix} 0 \\ 1 \end{pmatrix} \equiv 1_{classical} \tag{2.1.2}$$

$$\tag{2.1.3}$$

It is important to note the structure of this Hamiltonian (Equation. 1.2.1). Δ is fixed, a constant of the system. ϵ, in contrast, can be set by through the applied magnetic field. Thus we can adjust how similar $\hat{H}$ is to $\hat{\sigma}_z$ or $\hat{\sigma}_x$ through choice of ϵ. When $\epsilon \gg \Delta$, the cross term is negligible and the Hamiltonian is nearly proportional to $\hat{\sigma}_z$. In contrast, if $\epsilon \ll \Delta$, the cross term dominates and $\hat{H}$ is roughly proportionally to $\hat{\sigma}_x$. This implies that as $\epsilon \to 0$, the energy eigenstates transition from eigenstates of $\hat{\sigma}_z$ to eigenstates of $\hat{\sigma}_x$. Thus the computational states, which are eigenstates of $\hat{\sigma}_z$, will experience trivial time evolution when $\epsilon \gg \Delta$, but will mix when as $\epsilon \to 0$ (Fig. 2-1).

Based on the considerations from Section 1.2, it is clear that the ideal pulse to rotate a qubit is one period of a sinusoid. However, further simplification is possible while maintaining the key physics. First, note that since we are interested in strong driving, we require $A_{rf} \gg \Delta$ and $\epsilon_0 \gg \Delta$. Thus the computational states, $|0\rangle$ and

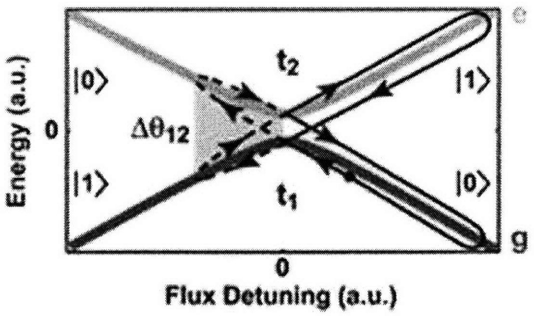

Figure 2-1: Systems starts in $|0\rangle$ on the lower right leg. It is then driven through the avoided crossing twice before returning to original location.

$|1\rangle$, are very nearly energy eigenstates except when $\epsilon_0 \approx A_{rf} \cos \omega t$. This allows us to approximate $\epsilon(t)$ with its second order Taylor expansion since there is no interaction as $\epsilon \to \pm\infty$. However, since interesting physics only occurs around avoided crossings, we shift to the second half of the cycle where the zeros occur ($\cos \omega t \to \cos(\omega t + \pi)$)

$$\epsilon'(t) = \epsilon_0 + \left(\frac{\omega^2}{2} t^2 - 1 \right) A_{rf} \tag{2.1.4}$$

We now see the problem reduces to the second order generalization of the Landau-Zener problem.

First, I will consider several limiting cases for the evolution. Our problem, like the Landau-Zener problem, can be characterized by the rate of change of ϵ about the zero crossing, $v = d\epsilon/dt$. Note that for parabolic driving, v differs only by sign at the two crossings.

First, take $\epsilon_0 > A_{rf}$. For this case, $\epsilon(t) \neq 0$ always, so the system is only weakly perturbed and remains in very nearly its initial state.

Next consider v small. The system is slowly brought to and away from the avoided crossing. Since the Hamiltonian changes slowly, the adiabatic theorem can be applied, giving that the system remains in the same quantum state over the course of the evolution. Thus, if the system were initialized to the ground state $|0\rangle$, it would remain in the ground state. As the avoided crossing is approached, the state slowly changes to $1/\sqrt{2}(|0\rangle + |1\rangle)$ and then to $|1\rangle$ as that becomes the ground state. Finally, the adiabatic return crossing brings the system back to the $|0\rangle$ state. This case applies to the case of ω very small.

The opposite case is v large. Once again, the system is initialized to the $|0\rangle$ state.

This time, however, the Hamiltonian is swept extremely rapidly through the avoided crossing. Because the interaction time, the time while $\epsilon/\Delta \ll 1$, is short, the system is unable to react and remains in the $|0\rangle$ state, which is now the first excited state. The return crossing is equally short, and again leaves the system in the $|0\rangle$ state.

Thus we see that for both large and small frequency driving, the system has only a small response. Notice that in one limit, the system remains fully in the ground state after the first avoided crossing, while in the other limit the system moves entirely into the first excited state after the first avoided crossing. The interesting region, where strong driving can occur, is the some small region between these two limits. Particularly, it is the region where it becomes possible to split the system into a precisely equal probability for $|0\rangle$ or $|1\rangle$ after the first crossing, where the crossing acts as a perfect 50-50 beam splitter.

In the 50-50 beam splitter regime, the final state is determined by the phase difference between the component remaining in $|0\rangle$ and the component switching into $|1\rangle$. To see this, consider the second avoided crossing. The two components will recombine, to form some superposition of $|0\rangle$ and $|1\rangle$. However, if the phases are aligned properly, the interference between the two paths will fully cancel the $|0\rangle$ or $|1\rangle$ component of the wave-function. If this occurs, the final state of the system will be either $|0\rangle$ or $|1\rangle$, depending one the interference.

We can make a preliminary guess to the location of the region of interest. The problem only has a few parameters: ω, ϵ_0, and Δ. ω is what we want to estimate, so it set it aside. Notice that the effect of ϵ_0 is to set the initial state of the Hamiltonian, namely to be large enough to make $\hat{h}(t = 0) \approx \epsilon_0 \hat{\sigma}_z$. This leaves Δ, so it is not unreasonable to guess that for strong driving, $\Delta \approx \hbar\omega$. I will not prove this, but later I will show evidence it is a correct.

A second way to approach the question of locating the strong driving region is through the Landau-Zener formula. Approximate each crossing of the parabola as a Landau-Zener crossing. Then the Landau-Zener formula gives us [9]:

$$P(L - Z\ transition) = e^{-2\pi\Gamma} = \frac{1}{2} \tag{2.1.5}$$

$$\Gamma = \frac{\Delta^2/\hbar}{|\frac{\partial}{\partial t}\epsilon|} \tag{2.1.6}$$

$$= \frac{\Delta^2/\hbar}{|A_{rf}\omega^2 t_{crossing}|} \tag{2.1.7}$$

Solving Equation 2.1.4 for the times of the crossings

$$t_{crossing} = \frac{\pm\sqrt{2}}{\omega}\sqrt{1 - \frac{\epsilon_0}{A_{rf}}} \approx \frac{\pm\sqrt{2}}{\omega} \tag{2.1.8}$$

Plugging this back in gives

$$\log\frac{1}{2} = -2\pi\Gamma \tag{2.1.9}$$

$$\log 2 = 2\pi\Gamma = \frac{2\pi\Delta^2\hbar}{\left|A_{rf}\omega^2\frac{\pm\sqrt{2}}{\omega}\right|} \tag{2.1.10}$$

$$= \frac{\sqrt{2}\pi\Delta^2}{\hbar A_{rf}\omega} \tag{2.1.11}$$

$$\frac{\Delta^2}{\hbar A_{rf}\omega} = \frac{\log 2}{\pi\sqrt{2}} \approx 0.156 \tag{2.1.12}$$

These considerations give a second condition, that $A_{rf}\omega\hbar$ be of order Δ^2, so both A_{rf} and ω should be of order Δ for strong driving.

2.2 Rotating Frame

The dynamics of the system can be visualized far more easily by switching into a rotating frame. In the appropriate rotating frame, the on diagonal term of the Hamiltonian disappears entirely, leaving only a time dependence on the cross term. This is achieved by choosing a new basis for the wave function [1].

$$|\psi\rangle = \hat{U}(t)\,|\psi'\rangle \tag{2.2.1}$$

This is substituted into Schrodinger's Equation (choosing units where $\hbar = 1$)

$$i\frac{d}{dt}|\psi\rangle = \hat{H}(t)\,|\psi\rangle \tag{2.2.2}$$

to give

$$i\frac{d}{dt}\hat{U}(t)\,|\psi'\rangle = \hat{H}(t)\hat{U}(t)\,|\psi'\rangle$$

$$i\hat{U}^\dagger(t)\frac{d}{dt}\hat{U}\,|\psi'\rangle = \hat{U}^\dagger(t)\hat{H}(t)\hat{U}(t)\,|\psi'\rangle$$

Expanding the left hand side

$$i\hat{U}^{\dagger}(t)\frac{d}{dt}\hat{U}\left|\psi'\right\rangle = i\hat{U}^{\dagger}(t)\left[\frac{d\hat{U}}{dt}\left|\psi'\right\rangle + \hat{U}\frac{d}{dt}\left|\psi'\right\rangle\right]$$

Rearranging terms

$$\begin{aligned} i\frac{d}{dt}\left|\psi'\right\rangle &= \left[\hat{U}^{\dagger}(t)\hat{H}(t)\hat{U}(t) - i\hat{U}^{\dagger}(t)\frac{d\hat{U}(t)}{dt}\right]\left|\psi'\right\rangle && (2.2.3) \\ &= \hat{H}'\left|\psi\right\rangle && (2.2.4) \end{aligned}$$

Now, through the appropriate choice of $\hat{U}$, it is possible to eliminate the diagonal terms of $\hat{H}'$. For

$$\begin{aligned} \hat{U}(t) &= exp\left\{\frac{i}{2}\ \delta\theta(t)\ \hat{\sigma}_z\right\} && (2.2.5) \\ \delta\theta(t) &= \int_0^t \epsilon(t')dt' = \epsilon_0 t + \frac{A}{\omega}\sin\omega t && (2.2.6) \end{aligned}$$

we find

$$\begin{aligned} \hat{H}' &= -\frac{1}{2}\begin{pmatrix} 0 & \Delta e^{\delta\theta(t)} \\ \Delta e^{-\delta\theta(t)} & 0 \end{pmatrix} && (2.2.7) \\ & && (2.2.8) \end{aligned}$$

Note that $\hat{U}(t)$ represents a rotation about the the z-axis, so $\left|\psi'\right\rangle$ differs from $\left|\psi\right\rangle$ by only a relative phase, which is not measurable. Thus we can use $\left|\psi'\right\rangle$, with evolution given by Equation 2.2.4, to understand the evolution of $\left|\psi\right\rangle$.

2.3 Experimental Setup

Our work was supported by experiments by Professor Terry Orlando's group at the Materials Processing Center at MIT. As mentioned earlier, the setup is a superconducting flux qubit, the state of which is read with a SQUID. The device, custom manufactured an MIT's Lincoln Laboratories, places the qubit and SQUID together on a single circuit board [7].

The qubit consists of a tiny, superconducting loop interrupted by three Josephson

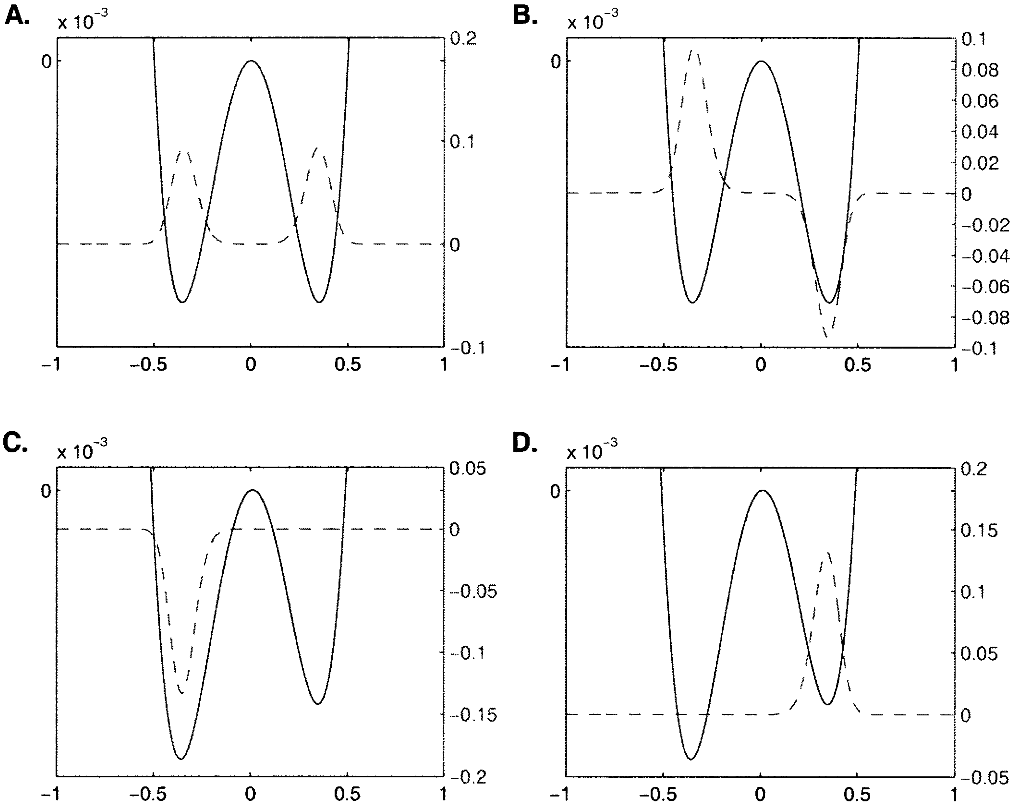

Figure 2-2: A and B show the first and second eigenstates of a symmetric potential with a double harmonic well. Note how each takes the form of a pair of Gaussians. C and D show the first and second eigenstates of an asymmetric double harmonic well. Note how each is a single, localized Gaussian.

Junctions. These junctions alter the Hamiltonian of the system, giving it a hilly, periodic structure. Luckily, this extremely complex system can safely be simplified using the tight binding model, where it is assumed the state is bound in one of the valleys of the Hamiltonian. However, the valleys are not so simple. Each valley consists of two separated local minima, and the system is effectively constrained to the two regions. Each local minima may be approximated well as a harmonic well, so ultimately the Hamiltonian reduces to two, adjacent, harmonic wells (Figure 2-2). The ground states of the harmonic wells, for reason discussed shortly, are generally the only states that need to be considered and can be modeled as two-state system, like the spin of an electron.

Interestingly, the intra-well relaxation time is rapid while the inter-well relaxation is slow. Since the intra-well relaxation is fast, the system can be assumed to always be in the ground state of one of the two wells; any excitations quickly decay back to the local ground state. This has proven to be an extremely useful feature for cooling the qubit [8], though it can lead to complex behavior when the system is coherently driven to higher energy states.

The slow inter-well relaxation is fortunate, as the system would make a poor qubit if it quickly decayed from one computational state to another, erasing the value stored in the qubit.

Chapter 3

Protocol

We propose a new protocol to rotate a qubit. In contrast to the standard technique relying on Rabi oscillations in the weak driving regime, we instead use the strong driving regime. The energy gap between the two states is swept parabolically, passing through the avoided crossing twice before returning to the initial energy gap (Fig. 2-1). We will show strong driving can achieve any arbitrary rotations.

3.1 Simulation

Because of the non-trivial time evolution of the Hamiltonian, it is impossible to calculate the final state analytically. Rather, I simulated the time evolution of the system numerically. All simulations were completed using standard functions in MATLAB. (Code can be found in Appendix A.)

Several types of simulations and presentations were carried out and evaluated to understand the dynamics of the system and to best present the results.

All simulations relied on the Bloch sphere representation of the two-state system. Though of the same computation complexity as the simulation of a complex 2-vector, I find the Bloch sphere approach to be far more intuitive. Furthermore, it allows results to plotted directly, rather than requiring additional processing. Finally, the Hamiltonian can be understood more easily as an effective magnetic field acting on a quantum dipole than as an abstract operator.

All simulations hold Δ constant, as it is fixed for a given system. The constant

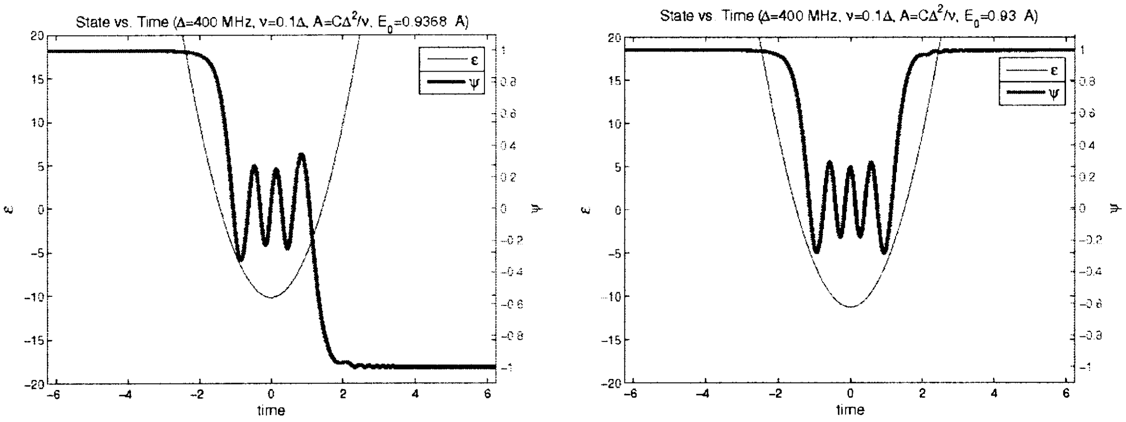

Figure 3-1: z component of ψ vs. time for two detunings. Note how dynamics only occur when ϵ is small (off scale, ϵ continues quadratically)

C,

$$C \equiv \frac{\pi\sqrt{2}}{\log 2} \approx 6.410 \tag{3.1.1}$$

is dimensionless and gives the ratio of $\hbar A_{rf}\omega$ to Δ^2. I expect to optimize the transition probability, as derived in Equation 2.1.12. Finally, $\hbar$ is taken to be 1.

3.1.1 Transition Probability vs. Time

The simplest plot is transition probability vs. time. Rather than plotting the transition probability itself, I simply plotted the z-component of the final Bloch vector, as this is proportional to the expectation value of the spin state (1 being a 100% likelyhood of $|0\rangle$, -1 a 100% likelyhood of $|1\rangle$). Requiring only one integration, these were extremely quick plots.

These simple line plots demonstrate how the system evolves in time for some particular set of parameters. Thus, while not useful for exploring parameter space for optimal regions, they are useful for understanding the underlying processes that give rise to the large scale structure seen in other plots, for example in Figure 3-1.

3.1.2 Bloch Vector vs. Time

Similar to transition probability vs. time, but now plotting the full Bloch vector in three dimensions against time. While difficult to appreciate as a static image, when

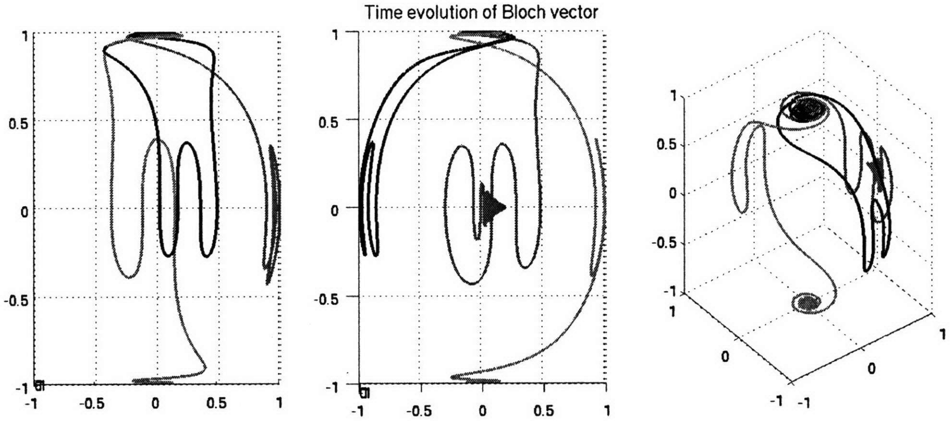

Figure 3-2: Time evolution of Bloch vector for 3 detunings. Three views of the same time evolutions, just from different angles.

dynamically rotated these plots give a good feel for the time evolution. It is extremely useful to perform these simulations in the rotating frame described in section 2.2 as the resulting trajectories are far simpler.

Several interesting features are visible in this plot as can be seen in Figure 3-2. First, by only changing the detuning the net rotation can be fully controlled, anywhere from 0 to π. More interesting is to notice how the system decides the rotation. For all three detunings, the time evolution begins with a jump to the $x - y$ plane. There, the vector oscillates momentarily before jumping to its final rotation. This can be understood as an interference pattern, the avoided crossing acting as a beam-splitter and the final state being decided by how the beams recombine and interfere at the second avoided crossing. Adjusting the detuning changes the phase difference between the two "beams", so an interference pattern emerges. Finally, note how the system spends most of its time in tight, nearly stationary spirals before and after the jump. This behavior confirms our prediction the system is only slightly affected when the energy gap between the states is large, the system only evolves when the energy gap is small.

3.1.3 Transition Probability vs. Detuning and Amplitude

Once the basic dynamics were understood by observing how the Bloch vector evolved with time, the next step was to find the region of parameter space that allowed for full *pi* rotations, the $50 - 50$ beam splitter regime. To do that, I explored the large-scale structure of the parameter space using plots varying both amplitude and detuning,

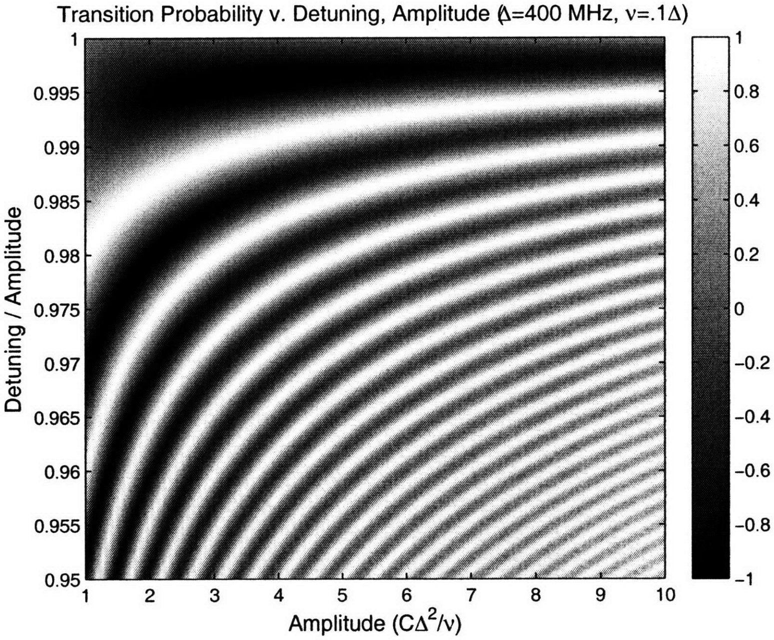

Figure 3-3: Final value of z component of ψ vs. Amplitude and the ratio of detuning to amplitude. Spin is fully flipped at $(1.585 \pm .005, 0.9765 \pm .00025)$ and $(3.464 \pm .005, 0.9960 \pm .00025)$

showing final transition probability as a color.

For a fixed detuning, the smallest amplitude for which strong driving is conceivable is $A_{rf} = \epsilon_0$, as noted earlier. This suggests that instead of plotting the raw detuning along the y-axis, the ratio of detuning to amplitude be plotted. Under these conventions, the first interactions for any amplitude will all be aligned vertically, since they all occur at a ratio of 1.

Examining Figure 3-3, we see there are two primary regions of interest regions of interest in the search for a set of parameters that give a full π qubit rotation: around the center of the first dark band from the top, and near the left side of the second line from the top. Out side of these two regions, the simulation shows a *pi* rotation is not possible. Using basic MATLAB functions I found the points of minimal expected value for the z component of o the Bloch vector, the points where the Bloch vector is flipped as nearly as possible from the $+\hat{z}$ direction to the $-\hat{z}$ direction. For both of the regions of interest, a full π rotation was found to be possible.

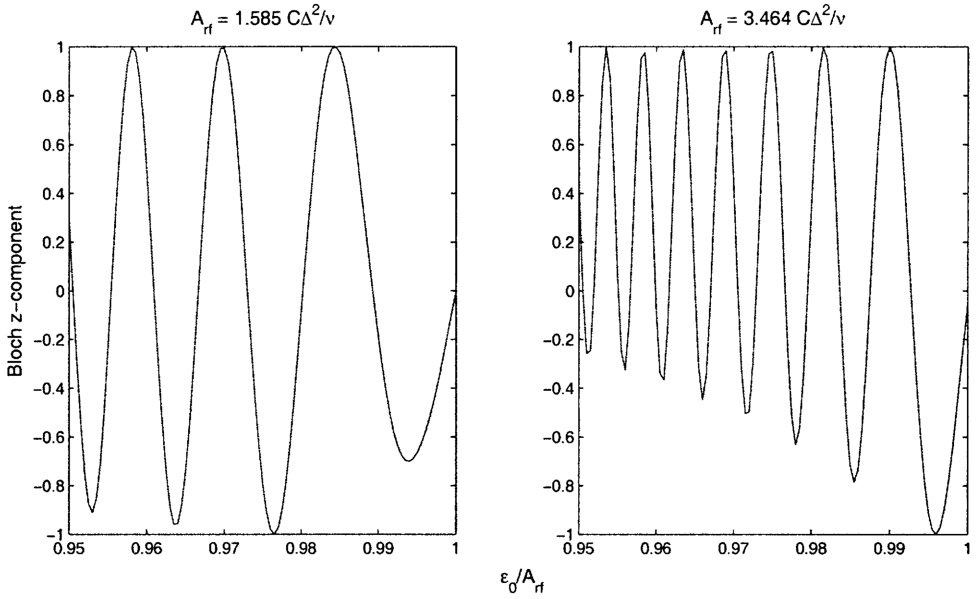

Figure 3-4: Final value of z component of ψ vs. detuning for two amplitudes. Note the range extends to -1 in both, indicating a full π rotation.

3.1.4 Transition Probability vs. Detuning

A slice out of the previous plot, plots of transition probability against detuning are useful for understanding how the rotation is affected by varying detuning, making the Bessel function dependence clear [6]. Amplitude and frequency are held constant, and then for each of a range of detunings ϵ_0, the full time evolution is simulated. The final transition probability is plotted against detuning.

The parameter space tend to be structured with sharp resonances in detuning. This behavior is visible in Figure 3-3, but is made even more clear by choosing a fixed amplitude, so transition probability can be seen on the $y-$axis rather than as a color, as in Figure 3-4. These resonances make it especially important to find precisely the values for detuning that maximize transition probability to be able to perform full π rotations. These plots allow for this, by giving high resolution slices of parameter space.

3.1.5 Final Bloch vector vs. Detuning

To explore what region of the Bloch sphere is traversable via strong driving, I plotted the final position of the Bloch vector after a cycle against detuning. In this plot, it is extremely easy to see by what angles a qubit can be rotated. The ideal, which

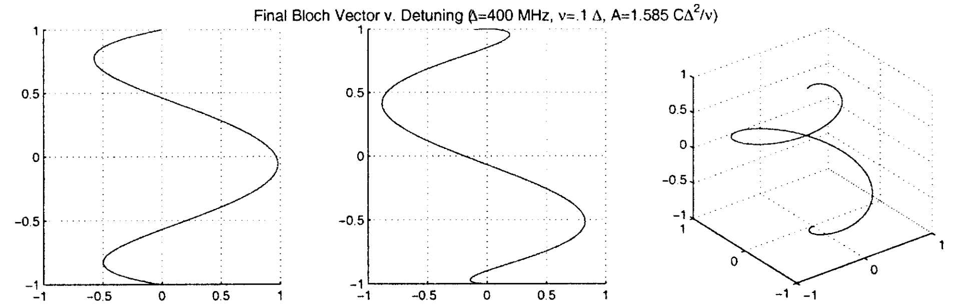

Figure 3-5: Final value of Bloch vector vs. detuning. All three figures show the same plot but from different angles.

turns out to be the case, is the line formed by the final Bloch sphere vector varying detuning is continuous and extends from the $+\hat{z}$ to $-\hat{z}$, though it only reaches $-\hat{z}$ for some choices of A_{rf}. This behavior is visible in Figure 3-5.

3.1.6 Transition Probability vs. Time and Detuning

This plot requires an identical calculation to the plot describe in Section 3.1.4, though the presentation is very different. Rather than focusing on a final value of the evolution, we use this plot to understand on a broad level how the detuning affects the time evolution. A second feature of this type of plot is it easily allows theoretical predictions to be compared to experimental results (Figures 3-6, 3-7).

3.2 Experiment

Preliminary work was done to verify the model experimentally. The basic model, simplifying the double harmonic well as a two state system, is well verified for weak, large amplitude driving [6]. Here we attempt to verify the model continues to hold for strong driving.

When I began my work, the experimental apparatus had no fine control over the duration over which rf radiation was applied to the qubit, so only long, time averaged affects could be quantified. This did allow some predictions from the theoretical models to be tested, but not the details of the time evolutions.

Advances in the experimental setup enabled us to verify the model for strong driving. Specifically, controls were added to very precisely set the start and stop time of the driving radiation. This allowed for very short pulses, even down to fractions

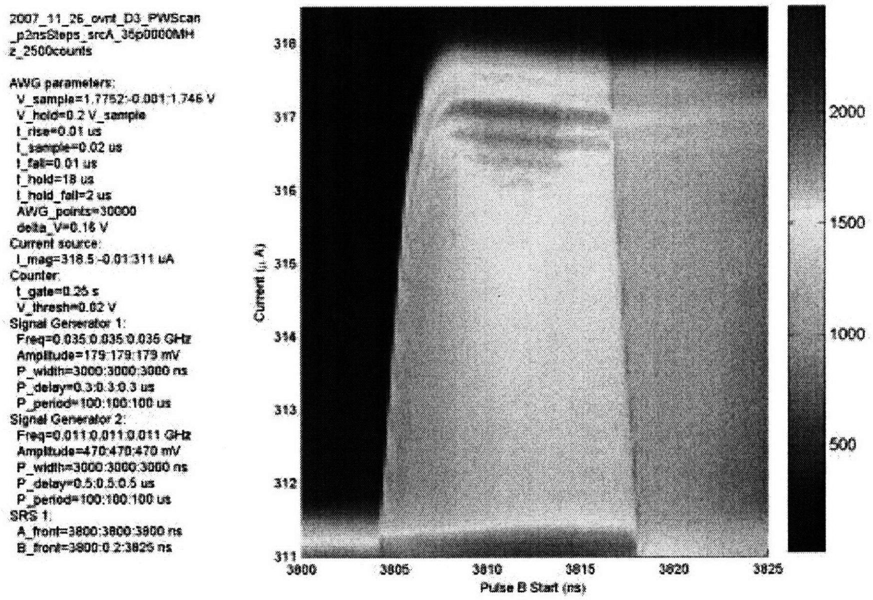

```
2007_11_26_ovnt_D3_PWScan
_p2nsSteps_srcA_35p0000MH
z_2500counts

AWG parameters:
  V_sample=1.7752:-0.001:1.746 V
  V_hold=0.2 V_sample
  t_rise=0.01 us
  t_sample=0.02 us
  t_fall=0.01 us
  t_hold=18 us
  t_hold_fall=2 us
  AWG_points=30000
  delta_V=0.18 V
Current source:
  I_mag=318.5:-0.01:311 uA
Counter:
  t_gate=0.25 s
  V_thresh=0.02 V
Signal Generator 1:
  Freq=0.035:0.035:0.035 GHz
  Amplitude=179:179:179 mV
  P_width=3000:3000:3000 ns
  P_delay=0.3:0.3:0.3 us
  P_period=100:100:100 us
Signal Generator 2:
  Freq=0.011:0.011:0.011 GHz
  Amplitude=470:470:470 mV
  P_width=3000:3000:3000 ns
  P_delay=0.5:0.5:0.5 us
  P_period=100:100:100 us
SRS 1:
  A_front=3800:3800:3800 ns
  B_front=3800:0.2:3825 ns
```

Current (μA)
318
317
316
315
314
313
312
311
3800
3805
3810
3815
3820
3825
Pulse B Start (ns)
2000
1500
1000
500

Figure 3-6: Experimental results. Detuning (y-axis) and time (x-axis) against transition probability (color)

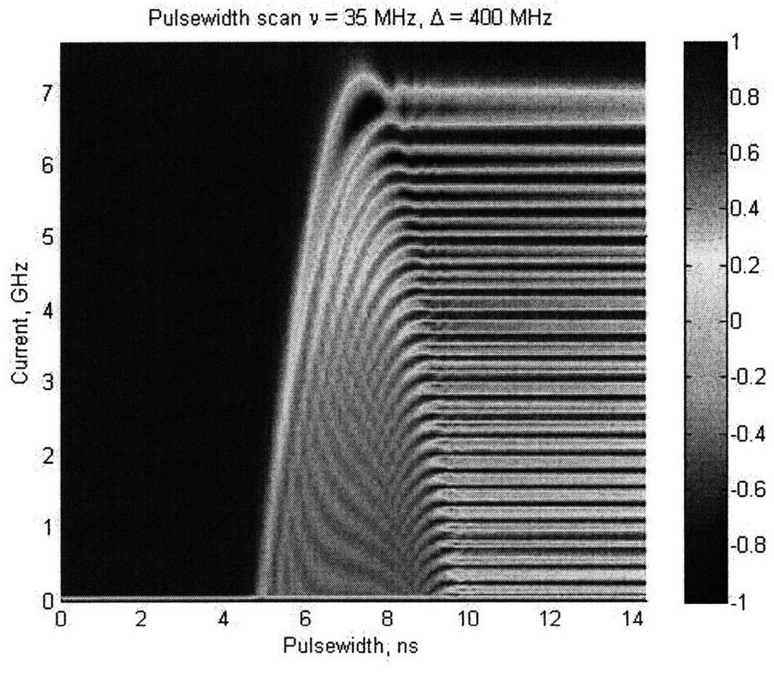

Figure 3-7: Simulation results. Detuning (y-axis) and time (x-axis) against transition probability (color). Note that colors are reversed relative to experimental plot

of a period. With such precise control, it was possible to examine how the qubit evolved over the course of one period of driving (Figure 3-6). These results were then compared with the model's predictions (Figure 3-7).

The strong qualitative correspondence between the experimental data and the theoretical prediction strongly supports the model. Furthermore, this fit has the added benefit of allowing us to characterize the parameters of the experiment. The only unknown parameter for the experiment was Δ, so by comparing the expected evolution of the system for various values of Δ we were able to find the best fit, $\Delta \approx 400$ MHz (in units where $\hbar = 1$).

3.3 Pulse Shape Variations

To confirm the robustness of the protocol, simulations were completed for various waveforms besides a simple parabola, as can be seen in Figure 3-8.

An obvious sample waveform was one period of a sine wave. The parabolic shape that was the focus of the work originated as an approximation to half of a sine wave, so it was natural to check how well the results translated back to the original function of interest. The exact function that was Taylor expanded to get a parabolic waveform was used, namely $\epsilon(t) = \epsilon_0 - A_{rf}\cos(\omega t)$ As can be clearly seen comparing Figure 3-3 to Figure 3-8, which use a parabolic and true cosine pulse, respectively, the parameter space has a very similar structure for either waveform.

A second function tried was a triangular pulse. The function was defined to be even and tangent to the parabolic function at the zero crossings.

$$\epsilon_{lin}(t) = 2(\epsilon_0 - A) + A\sqrt{2 - 2\epsilon_0/A}\,|x| \tag{3.3.1}$$

This is a significantly different functional form than Equation 2.1.4, but as can be seen in Figure 3-9, has remarkablbly similar structure. Again horizontal bands form with larger transition probability for lower amplitude. The fine structure is, however, noticably different. This is because the fine structure arises from the interference between the two paths after the first avoided crossing. Since the linear paths are very different from the parabolic paths far from the crossings, the interference pattern is different.

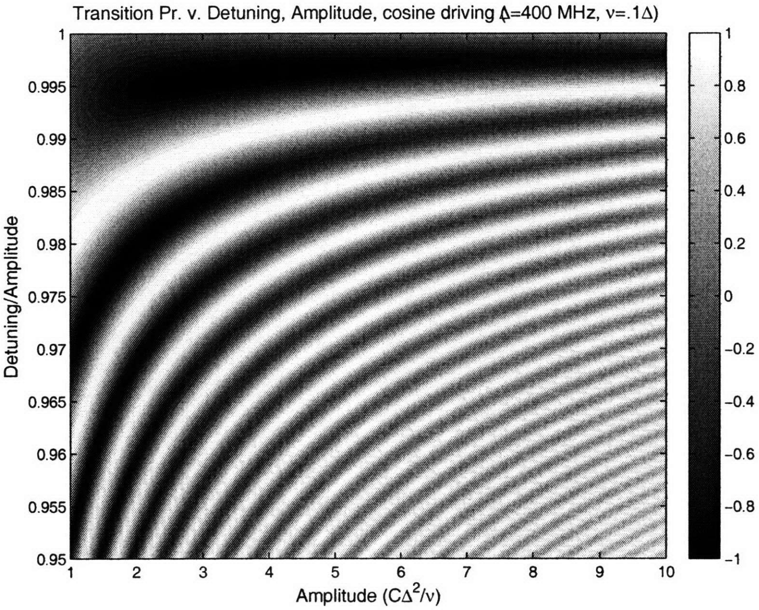

Figure 3-8: Final value of z component of ψ vs. Amplitude and the ratio of detuning to amplitude. Here driven by a true cosine waveform

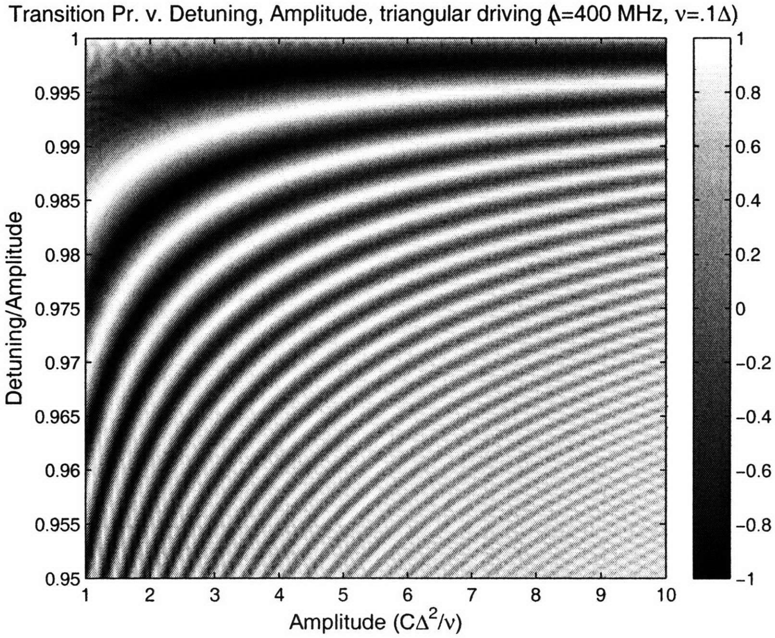

Figure 3-9: Final value of z component of ψ vs. Amplitude and the ratio of detuning to amplitude. Here driven by a triangular waveform.

Chapter 4

Conclusion

Strong driving was found to be an effective protocol for qubit manipulation. Through theoretical consideration a region of parameters space was discovered that allows for arbitrary SU2 rotations, and this prediction was confirmed through numerical simulations. Furthermore, the simulations have also shown strong driving is robust against variations in the waveform of the driving field.

The obvious advantage of strong driving is reduced interaction time, but it is not the only advantage. An added benefit of strong driving over weak driving is improved stability. The rotation realized through weak driving is a linear function of driving time. In contrast, our protocol rotates the qubit in discrete steps, so rotation angle is robust against small changes to driving time. Furthermore, π rotations are extrema of the parameter space, so to first order the rotations are robust against small variation in the parameters.

As noted earlier,the strong driving technique suggested here is the natural way to manipulate a flux qubit. Given the advantages of flux qubits for the implementation of a full quantum computer, our protocol deserves further study, especially in regard to its application to quantum computation. While the basics of the protocol have been explored, several important questions remain unanswered, two of which are touched on here.

Firstly, the magnitude of the speed improvement over weak driving needs to be quantified. This is a complex question as the two techniques largely rely on different parameters, but it is important to know before pursuing either further.

Secondly, and perhaps more a question of engineering than physics, is, on a chip contain many qubits, whether an individual qubit can be driven without disturbing the others. A possible solution to this problem is to have a dedicated inductor for each qubit to slightly alter the detuning and thereby affect whether or not in couples to the driving field, though again further study is warranted.

Appendix A

MATLAB Scripts

A.1 evolve.m

```
function final = evolve(E_mult, o_mult, A_mult)
%EVOLVE Plot time evolution of z-component of psi
%   hbar = 1

  C = (log(2)/(pi*sqrt(2)))^-1; % Constant coming from Landau-Zener
  Delta = 2*pi*.4; % Avoided crossing, GRad/sec

  final = zeros([3, length(E_mult) length(o_mult) length(A_mult)]);

  for oIter = 1:length(o_mult)
    Omega = o_mult(oIter) * Delta; % Driving Frequency, GRad/sec
    Freq = Omega/(2*pi); % Driving Frequency, GHz
    t_start = -.25/Freq; % ns
    t_stop = .25/Freq; % ns

    for aIter = 1:length(A_mult)
      A = A_mult(aIter)*C*Delta^2/Omega; % Driving Amplitude, GRad/sec

      for eIter = 1:length(E_mult)
        E0 = E_mult(eIter)*A;
        norm=(Delta^2+E0^2)^(-0.5);
        y0=[norm*Delta, 0, norm*E0];

        [t y] = ode45(@plot_rhs, [t_start t_stop], y0,[], ...
                      E0, Delta, A, Omega);
        final(:,eIter, oIter, aIter) = y(end,:);

% Uncomment for Transition Probability vs. Time plot
%{
        figure
        ax = plotyy(t, E(t,E0,Delta,A,Omega), t, y(:,3));
        xlim(ax(1),[min(t) max(t)]);
        xlim(ax(2), [min(t) max(t)]);
%}
      end
    end
  end

  final = squeeze(final);
end
function dmdt = plot_rhs(t,y,E0,Delta,A,Omega)
  w = [ Delta;
        0;
        E(t, E0, Delta, A, Omega)];

  dmdt = [y(2)*w(3)-y(3)*w(2);  % just cross(y,w), but faster
          y(3)*w(1)-y(1)*w(3);  % since uses w(2) = 0
          y(1)*w(2)-y(2)*w(1) ];
end
function energy = E(t, E0, Delta, A, Omega)
  % Uncomment desired waveform
  energy = E0 - A * (1 - .5*(Omega*t).^2); % parabolic
  % energy = E0 - A*cos(Omega*t); % cosine
  % energy = 2*(E0-A) + A*sqrt(2-2*E0/A)*abs(Omega*t); %linear
end
```

A.2 final.m

```
function[  x,y,z, t,e_vals  ] = final(num, A, Omega)
%FINAL Plot final state vs detuning
%  Evaluates Bloch evolution for range of detunings,
%  plots transition probability or location on Block sphere

  e_min = 0.95;          % Min Detuning, Units of A
  e_max = 1.00;          % Max Detuning, Units of A
  e_vals = linspace(e_min, e_max, num);

  r = evolve(e_vals, Omega, A);
  x = r(1,:);
  y = r(2,:);
  z = r(3,:);

% Transition Probability vs. Detuning plot
  figure;
  h = plot(e_vals, z);
  title(['Final Z position']);
  xlabel('Detuning (units of A)'); ylabel('Z');
  xlim([e_min e_max]); ylim([-1 1]);

% Uncomment for Final Bloch vector vs. Detuning plot
%{
  figure;
  h = plot3(x, y, z);
  title(['Bloch trajector']);
  xlim([-1 1]); ylim([-1 1]); zlim([-1 1]);
%}
end
```

A.3 contour.m

```
function contour(num)
  Omega = .1;    % Driving Frequency, Units of Delta

  e_min = 0.95;            % Min Detuning, Units of A
  e_max = 1.00;            % Max Detuning, Units of A
  e_vals = linspace(e_min, e_max, num+1);

  a_min = 1.0;
  a_max = 10.0;
  a_vals = linspace(a_min, a_max, num);

  r = evolve(e_vals, Omega, a_vals);
  z = squeeze(r(3,:,:));

  figure
  [C, h] = contourf(a_vals, e_vals, z);
  set(h, 'LineStyle', 'none'); set(h, 'LevelStep', .1);
  title('Transition Pr. v. Detuning, Amplitude');
  xlabel('Amplitude (C\Delta^2/\nu)');
  ylabel('Detuning/Amplitude');
end
```

A.4 rotbloch.m

```
function [  x,y,z, t,e_vals  ] = rotbloch(o_mult, A_mult, e_num)
%ROTBLOCH Plot spin 1/2 evolution on block sphere in rotating frame
%  Lines show constant detuning, color shows time

  C = (log(2)/(pi*sqrt(2)))^-1; % Constant coming from Landau-Zener
  Delta = 2*pi*.4; % Avoided crossing, GRad/sec

  Omega = o_mult * Delta;
  Freq = Omega/(2*pi); % GHz
  A = A_mult*C*Delta^2/Omega; % GRad/sec

  e_min = 0.9695 * A; % GRad/sec
  e_max = 0.9765 * A; % GRad/sec
  e_vals = linspace(e_min, e_max, e_num);

  t_start = -0.25/Freq; % ns
  t_stop = 0.25/Freq;% ns
  t_num = 10000;
  t = linspace(t_start, t_stop, t_num);

  r = zeros(3, t_num, e_num);
  for j = 1:e_num
    E0 = e_vals(j);
    norm=(Delta^2+E0^2)^(-0.5);
    y0=[norm*Delta, 0, norm*E0];

   [t y] = ode45(@rot_rhs, t, y0,[], E0, Delta, A, Omega);

    r(1, :, j) = y(:,1)';
    r(2, :, j) = y(:,2)';
    r(3, :, j) = y(:,3)';
  end
  xr = squeeze( r(1,:,:) )';
  yr = squeeze( r(2,:,:) )';
  zr = squeeze( r(3,:,:) )';

  b = ones(size(t));
  c = kron(b', e_vals');

  % Bloch Vector vs. Time plot
  figure;
  h = mesh(xr, yr, zr, c, 'MeshStyle', 'row', 'FaceAlpha', 0);
  xlim([-1 1]); ylim([-1 1]); zlim([-1 1]);
  title('Evolution in rotating frame');

% Uncomment for Transition Probability vs. Time and Detuning plot
%{
   figure;
   [c, ch3] = contourf(t, e_vals/2/pi, zr);
   set(ch3, 'linecolor', 'none');
   title(['Pulsewidth scan']);

   xlabel('Pulsewidth, ns');
   ylabel('Current, GHz');
%}
end

function dmdt = rot_rhs(t,y,E0,Delta,A,Omega)
  w = [ Delta * cos( theta(t,E0,A,Omega) );
        -Delta * sin( theta(t,E0,A,Omega) );
        0];

  dmdt = [y(2)*w(3)-y(3)*w(2);
          y(3)*w(1)-y(1)*w(3);
          y(1)*w(2)-y(2)*w(1) ];
end
```

```
function th = theta(t,E0,A,Omega)
  t0 = -.5*pi/Omega; % = .25/Freq

  % Evolution using harmonic driving
  th = E0*(t-t0) - A/Omega*(sin(Omega*t) - sin(Omega*t0));

  % Evolution using parabolic driving
% th = E0*(t-t0) - A/Omega*(parasin(Omega*t,-.5*pi) ...
%            - parasin(Omega*t0,-.5*pi));
end

function y = parasin(x, x0)
  y = (x-x0) - (1./6.)*(x.^3 - x0^3);
end
```

Bibliography

[1] S. Ashhab, J. R. Johansson, A. M. Zagoskin, and Franco Nori. Two-level systems driven by large-amplitude fields. *Physical Review A*, 75:063414, 2007.

[2] I. Chiorescu, Y. Nakamura, C. J. P. M. Harmans, and J. E. Mooij. Coherent quantum dynamics of a superconducting flux qubit. *Science*, 299:1869, 2003.

[3] David P. DiVincenzo. The physical implementation of quantum computation, 2000.

[4] Richard Feynman. Simulating physics with computers. *International Journal of Theoretical Physics*, 21(6&7):467–488, 1982.

[5] M.A. Nielsen and I.L. Chuang. *Quantum Computation and Quantum Information.* Cambridge University Press, 2000.

[6] W.D. Oliver, Y. Yu, J.C. Lee, K.K. Berggren, L.S. Levitov, and T.P. Orlando. Mach-Zehnder Interferometry in a Strongly Driven Superconducting Qubit, 2005.

[7] TP Orlando, JE Mooij, L. Tian, C.H. van der Wal, LS Levitov, S. Lloyd, and JJ Mazo. Superconducting persistent-current qubit. *Physical Review B*, 60(22):15398–15413, 1999.

[8] S.O. Valenzuela, W.D. Oliver, D.M. Berns, K.K. Berggren, L.S. Levitov, and T.P. Orlando. Microwave-Induced Cooling of a Superconducting Qubit, 2006.

[9] C. Wittig. The landau-zener formula. *Journal of Physical Chemistry B*, 109(17):8428–8430, 2005.